Cancer Cell
Article

# Hematogenous Metastasis of Ovarian Cancer: Rethinking Mode of Spread

Sunila Pradeep,[1] Seung W. Kim,[2] Sherry Y. Wu,[1] Masato Nishimura,[1] Pradeep Chaluvally-Raghavan,[3] Takahito Miyake,[1] Chad V. Pecot,[4] Sun-Jin Kim,[2] Hyun Jin Choi,[1] Farideh Z. Bischoff,[10] Julie Ann Mayer,[10] Li Huang,[2] Alpa M. Nick,[1] Carolyn S. Hall,[5] Cristian Rodriguez-Aguayo,[6,7] Behrouz Zand,[1] Heather J. Dalton,[1] Thiruvengadam Arumugam,[2] Ho Jeong Lee,[2] Hee Dong Han,[1,7,11] Min Soon Cho,[8] Rajesha Rupaimoole,[1] Lingegowda S. Mangala,[1,7] Vasudha Sehgal,[3] Sang Cheul Oh,[3,12] Jinsong Liu,[9] Ju-Seog Lee,[3] Robert L. Coleman,[1] Prahlad Ram,[3] Gabriel Lopez-Berestein,[6,7] Isaiah J. Fidler,[2] and Anil K. Sood[1,2,7,*]
[1]Department of Gynecologic Oncology and Reproductive Medicine
[2]Department of Cancer Biology
[3]Department of Systems Biology
[4]Department of Thoracic, Head, and Neck Medical Oncology
[5]Department of Surgical Oncology
[6]Department of Experimental Therapeutics
[7]Center for RNA Interference and Non-coding RNA
[8]Department of Benign Hematology
[9]Department of Pathology
University of Texas M.D. Anderson Cancer Center, Houston, TX 77030, USA
[10]Biocept Inc., San Diego, CA 92121, USA
[11]Department of Immunology Laboratory, School of Medicine, Konkuk University, Chungju 380-701, South Korea
[12]Division of Hemato-Oncology, Department of Internal Medicine, Korea University Medical Center, Korea University College of Medicine, Seoul 136-705, Korea
*Correspondence: asood@mdanderson.org
http://dx.doi.org/10.1016/j.ccr.2014.05.002

## SUMMARY

**Ovarian cancer has a clear predilection for metastasis to the omentum, but the underlying mechanisms involved in ovarian cancer spread are not well understood. Here, we used a parabiosis model that demonstrates preferential hematogenous metastasis of ovarian cancer to the omentum. Our studies revealed that the ErbB3-neuregulin 1 (NRG1) axis is a dominant pathway responsible for hematogenous omental metastasis. Elevated levels of ErbB3 in ovarian cancer cells and NRG1 in the omentum allowed for tumor cell localization and growth in the omentum. Depletion of ErbB3 in ovarian cancer impaired omental metastasis. Our results highlight hematogenous metastasis as an important mode of ovarian cancer metastasis. These findings have implications for designing alternative strategies aimed at preventing and treating ovarian cancer metastasis.**

## INTRODUCTION

Most patients identified with newly diagnosed ovarian cancer present with widespread metastases, and this tumor burden remains a major clinical challenge (Naora and Montell, 2005). Although epithelial ovarian cancer is widely believed to metastasize via direct surface spread aided by the peritoneal circulation, the distribution of metastasis from the primary tumor is not completely random; a predilection for early and robust omental implantation is consistently identified. The omentum is a large

### Significance

Ovarian cancer has been thought to spread primarily via intraperitoneal "seeding." However, the presence of circulating tumor cells (CTCs) and abundant tumor cells in the omental vasculature prompted us to consider an alternative route of metastasis. Here, using a parabiosis model where the skin of mice was fused surgically from the shoulder to the hip joint, we demonstrated that ovarian CTCs implant and grow in the omentum preferentially and subsequently spread to other peritoneal surfaces. ErbB3 expression in the CTCs and NRG1 in the omentum is the axis responsible for hematogenous metastasis to the omentum. These findings represent a paradigm shift in our understanding of ovarian cancer metastasis and have substantial implications for clinical management of this frequently metastatic disease.

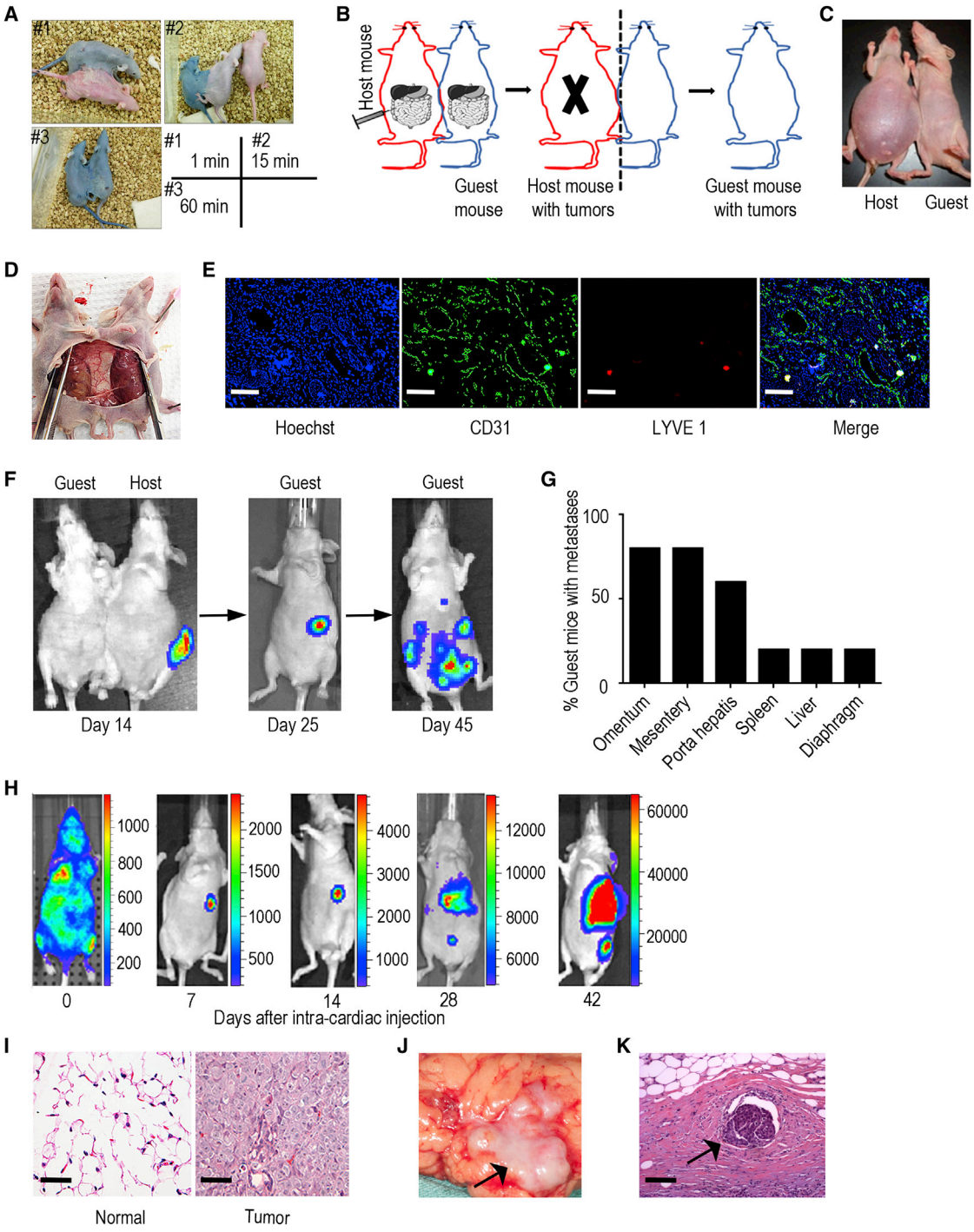


**Figure 1. Parabiosis Model Shows that Omental Tumor Cells Can Metastasize Hematogenously**

(A) Surgically attached parabionts 1 (#1), 15 (#2), and 60 (#3) minutes after the host mice were injected with 1% Evan's blue dye.

(B) Diagram of the parabiosis model where two mice were surgically joined. After 2 weeks, parental ovarian cancer cells were injected into the host mice. Once they became moribund, the parabionts were separated, and the host mice were euthanized. The guest mice were further observed.

(C) Pictured is a moribund parabiont where SKOV3-OM1 cells were recycled (SKOV3-OM3) in the immunodeficient parabiosis model.

(D) The dissected abdominal cavity of a representative parabiont 2 weeks after anastomosis.

(E) CD31 and LYVE1 antibody staining of sections of the skin from between the anastamosed mice. Scale bars represent 100 μm.

(F) Bioluminescence imaging of tumor cells injected into the ovary of the host mice on day 14 and of the guest mice of separated parabionts on days 25 and 45.

(G) Localization of metastatic nodules was quantified and plotted.

(H) Bioluminescence imaging of recycled SKOV3-OM3 cells introduced into the circulation via intracardiac injection. The color scale depicts the photon fluxes emitted from the tumor cells.

*(legend continued on next page)*

fatty structure, which arises off the greater curvature of the stomach, attaches loosely to the transverse colon, and drapes over the lower abdomen and pelvis. However, the sequential processes and mechanisms involved in metastasis to this organ are not well understood.

Passive and repetitive exposure of the peritoneal cavity to exfoliated cancer cells has long been thought to be the dominant source of gross peritoneal disease. However, at initial diagnosis, many patients have retroperitoneal or distant metastases (e.g., hepatic and pulmonary parenchyma) (Akin et al., 2008; Castadot et al., 2005; Lim et al., 2009). Moreover, even within the peritoneal cavity, the presence of submesothelial disease raises the possibility of alternate routes of metastasis. We and others have demonstrated that ovarian cancer patients have circulating tumor cells (CTCs) in the blood (Pecot et al., 2011; Phillips et al., 2012), but the biological significance of CTCs in ovarian cancer patients is not well understood. Previous clinical studies of peritoneovenous shunts showed that despite large quantities of CTCs, disease was predominantly confined to the abdomen (Tarin et al., 1984). These clinical observations prompted us to investigate whether ovarian cancer cells fundamentally lack the ability to metastasize hematogenously or whether a blood-borne route might lead to preferential metastasis to abdominal organs.

## RESULTS

### Epithelial Ovarian Cancer Cells Are Able to Metastasize to the Omentum Hematogenously

To determine the metastatic patterns of CTCs in ovarian cancer, we established a parabiosis model. In this model, the skin of female mice was excised from the shoulder to the hip joint, and pairs of mice were then surgically anastomosed (n = 20 pairs). The parabionts were wrapped with an elastic band to relieve wound tension and to prevent twisting. Two weeks after anastomosis, the "host" parabiont mice were injected with 100 μl of 1% Evan's blue dye intravenously. Within 15 min, the dye was noted in the "guest" mice, which confirms the establishment of a common circulation (Figure 1A).

Next, we sought to determine whether tumor cells injected into the peritoneal cavity of each host mouse could hematogenously metastasize to the corresponding guest mouse. Figure 1B shows a schematic representation of parabiosis, whereby each host mouse was injected with SKOV3ip1 ovarian cancer cells into the abdominal cavity. Once the host mice became moribund (Figure 1C), the parabionts were separated (Figure S1A available online), and the host mice were euthanized. Tumor development and patterns of metastasis were then observed in the guest mice (Figure S1B). In host mice, 15 of 15 mice had metastasis in the omentum, and in guest mice, 8 of 15 mice had metastasis (Table S1) within the omentum or mesentery. The cell lines derived from omental tumors in guest mice were termed SKOV3-OM1 cells. These cells were subsequently recycled through parabiosed mice and were denoted as SKOV3-OM3 subpopulations. Figure 1D shows that the abdominal cavities of the parabionts are intact and not directly connected. To determine whether paired mice in the parabiosis model share vasculature, sections from the shared skin of parabiosis mice were stained for both blood (CD31) and lymphatic (LYVE1) vessels. The staining shows that the paired mice shared blood but not lymphatic vessels (Figure 1E).

We next asked whether ovarian cancer can spread from the primary site (i.e., ovary) in the host mouse via the circulatory system to the omentum of the guest mouse. Two weeks after anastomosis, the host mice were injected with tumor cells directly into the ovary (ten pairs). In this model, the parabionts were separated 2 weeks following tumor cell injection, at which point only primary tumor was present in the host mice (Figure 1F). We monitored tumor growth in the guest mice every week using bioluminescence imaging. Following separation, imaging analysis on day 25 showed presence of tumor in the omentum prior to spreading to other organs in the guest mice (Figure 1F). To determine whether micrometastases might be present in other organs (ovary, mesentery, spleen, and liver) at this point, we performed a necropsy (five mice). No apparent microscopic metastases were found in these organs (Figure S1C) except omentum. We continued to monitor tumor growth in the other five mice until they became moribund (45–60 days after separation; Figure 1G; Figure S1D).

To further assess the ability of SKOV3-OM3 (luciferase-positive) cells to spread hematogenously, we injected these cells into the left ventricle of the heart and then performed longitudinal bioluminescence imaging. Following intracardiac injection, the tumor cells were rapidly distributed throughout the body (Figure 1H, day 0). Within 7 days, the entire bioluminescence signal had cleared except those infiltrated in the omentum. By day 28, tumors were visible in other organs (Figure S1E). Histological analysis confirmed that SKOV3-OM3 lesions replaced large areas of the omentum (Figure 1I). Because nude mice lack mature T-lymphocytes, we next used immune-competent mouse models to determine whether ovarian cancer could metastasize hematogenously in such models. For these experiments, we used IG10 cells in C57BL/6 mice, and similar findings to those described above were noted (Figure S1F). Specifically, the guest mice developed metastases within the omentum or mesentery (Figure S1G). To determine whether such metastases could occur in patients, we evaluated tissue samples from five patients with a primary tumor with an intact capsule (i.e., high-grade serous histology) and isolated omental metastasis (i.e., no gross or microscopic metastases elsewhere in the abdomen; Figure 1J). Histological assessment revealed extensive tumor cell deposits in blood vessels within the omentum (Figure 1K).

### Cells Prone for Omental Metastasis Have Elevated Levels of ErbB3

To identify potential mechanisms by which ovarian cancer cells metastasize to the omentum, we examined the differences in gene expression profiles between SKOV3ip1 and SKOV3-OM3 cells. To identify the most biologically relevant processes that

(I) Hematoxylin and eosin (H&E) staining of normal omentum and tumor omentum. Scale bars represent 50 μm.
(J) Omental metastasis in a patient with an isolated ovarian mass with an intact capsule.
(K) H&E staining of regions of the omentum without gross disease from a patient. Scale bar represents 100 μm.
See also Figure S1 and Table S1.

may drive the phenotype, we performed a network-based analysis of the gene expression data whereby the gene expression values and gene connectivity networks were used to identify the pathways and networks that were most significantly altered (Komurov et al., 2012a, 2012b, 2010). We analyzed the fold-change differences in gene expression between the two cell lines (Figures S2A and S2B) and found that a 1.5-fold cutoff encompassed the top 2.45% of the genes that were altered. All genes meeting this cutoff have significant p values. From the genes that were most downregulated, we observed that the EGFR-ErbB2 network had the greatest number of genes that were significantly downregulated. Therefore, we analyzed the *EGFR* family in greater detail. The heat maps in Figure 2A and Figure S2C show selected and all members of the *EGFR* family, respectively. The complete gene array data are included in Table S2. Of all the genes in the *EGFR* family, *ERBB3* and *NRG1*, which encodes the ERBB3 ligand neuregulin 1 (NRG1), were selected for further examination because their expression levels were significantly elevated in SKOV3-OM3 compared with SKOV3ip1 cells, an observation that is distinctly different from other members in this family (Figure 2A; Figure S2D). The phospho-RTK array also showed that ErbB3 phosphorylation was significantly increased in SKOV3-OM3 cells (Figure 2B). Therefore, we examined the ligand that could lead to phosphorylation of ErbB3 and found that *NRG1* expression was significantly increased. Results from these gene and phospho-RTK arrays were validated using quantitative real-time (qRT)-PCR (Figures S2E–S2K) and Western blot (Figure 2C) techniques, respectively. Of note, the expression of ErbB3 and ErbB4, as well as their corresponding phosphorylated forms, were all present at a higher level in SKOV3-OM3 compared with SKOV3ip1 cells. To examine the downstream signaling consequences of the ErbB3 pathway, we evaluated changes in phosphatidylinositol 3-kinase (PI3K)/AKT and Src phosphorylation levels in both cell lines after NRG1 stimulation. Both Src and PI3K/AKT phosphorylation levels were intrinsically higher in SKOV3-OM3 cells when compared with SKOV3ip1 cells and were further increased upon NRG1 stimulation (Figure 2D).

Because NRG1 is known to affect cytoskeletal reorganization (Adam et al., 1998), we used gold-labeled immunosorbent assay (G-LISA) to assess the activity of Rac1, a protein involved in cell migration. We found that NRG1 triggered Rac1 activation at a significantly higher rate in SKOV3-OM3 than in SKOV3ip1 cells (Figure 2E). Importantly, this induction of Rac1 by NRG1 stimulation could be abrogated by ErbB3, PI3K, or Src inhibition. To determine the role of Rac1 activation in the loss of tissue polarity, we seeded SKOV3ip1 and SKOV3-OM3 cells on a 3D, laminin-rich basement membrane (3DlrBM) and identified phenotypic effects of blocking ErbB3. When ErbB3 or its downstream effector PI3K was blocked, the polarity of SKOV3-OM3 cells was restored (Figure 2F). The downregulation of ErbB3 and pErbB3 in cells following αErbB3 treatment was validated by Western blot analysis (Figure S2L). Both pFak and phospho-p85, two important downstream effectors of ErbB3, were also downregulated in these αErbB3-treated cells (Figure S2M).

## Ovarian Cancer CTCs Have Strong ErbB3 Expression

We next sought to determine whether the differences in the gene signatures of SKOV3ip1 and SKOV3-OM3 cells indicate differences in the ability of these cells to undergo epithelial-mesenchymal transition (EMT). We found that several mesenchymal phenotype-related genes such as vimentin, *MMP3*, *COL1A*, *HMGA2*, and *HGF* were upregulated in the SKOV3-OM3 cells (Figure 3A). Moreover, negative EMT regulators (e.g., E-cadherin, *SFRP1*, *EFNA1*, and *SMAD7*) were downregulated in SKOV3-OM3 compared with SKOV3ip1 cells (Table S2). E-cadherin and vimentin expression were validated at both RNA and protein levels (Figure 3B; Figure S3A). Increased vimentin expression in SKOV3-OM3 cells was also confirmed via immunofluorescence staining in 3D cultures following NRG1 stimulation (Figure 3C). This increase was blocked by ErbB3 small interfering RNA (siRNA) treatment, indicating the role of ErbB3 in the EMT process (Figure 3D; Figure S3B). We further showed that both vimentin and E-cadherin are regulated by ErbB3 and PI3K (Figures S3C and S3D).

To further assess the role of ErbB3 in promoting hematogenous spread of ovarian cancer cells, we used a microfluidics-based device capable of capturing both CK-positive ($CK^+$) and CK-negative ($CK^-$) cells (Pecot et al., 2011). More than 95% of CTCs collected from mice bearing SKOV3-OM3 ovarian tumors were $ErbB3^+$ (Figures 3E–3G; Table S3). This is consistent with the finding that ErbB3 expression promotes EMT phenotype of cancer cells (Figure 3D). The level of $ErbB3^+$ CTCs was also found to be positively correlated with total tumor burden (Figure 3H). We also examined CTCs in the parabiosis model in both the host and guest mice, which showed an average of 52.3 CTCs/ml in the host compared with 7.4 CTCs/ml in the guest mice (Figure S3E). To determine whether $ErbB3^+$ CTCs could also be detected in ovarian cancer patients, we collected CTCs from nine patients and examined their ErbB3 expression. Consistent with our in vivo observations, more than 90% of CTCs from these patients were ErbB3-positive ($ErbB3^+$) (Figure S3F). Given that omentum is the primary site of metastasis, we sectioned and stained the omental tissue from five ovarian cancer patients using CD31 and ErbB3 antibodies. In all the sections examined, we found that the tumor cells within the blood vessels in the omentum have strong ErbB3 expression (Figure 3I). To examine the clinical relevance of tumoral ErbB3 expression, we next assessed the effect of ErbB3 on patient survival. In a cohort of 217 advanced-stage ovarian cancer patients, lower ErbB3 expression was significantly correlated with improved overall survival (median survival 3.15 versus 4.9 years, $p < 0.001$; Figures 3J and 3K). In univariate analysis, high ErbB3 expression was significantly associated with advanced stage at diagnosis ($p = 0.003$; Table S4). In multivariate analysis controlling for age, disease stage, histologic grade, and extent of cytoreduction, ErbB3 remained a significant independent factor for patient survival (Table S4). Supporting the hypothesis that ErbB3 expression facilitates metastatic disease, we found that ErbB3 expression was significantly higher in stage III–IV tumors when compared with stage I–II tumors.

## Loss of ErbB3 Inhibits Metastasis in Mouse Models of Ovarian Cancer

To examine the functional role of ErbB3 in hematogenous metastases, we used our well-characterized methods for systemic delivery of siRNA to tumor and stromal cells in vivo (Ahmed et al., 2010; Landen et al., 2005). Using the dioleoylphosphatidylcholine

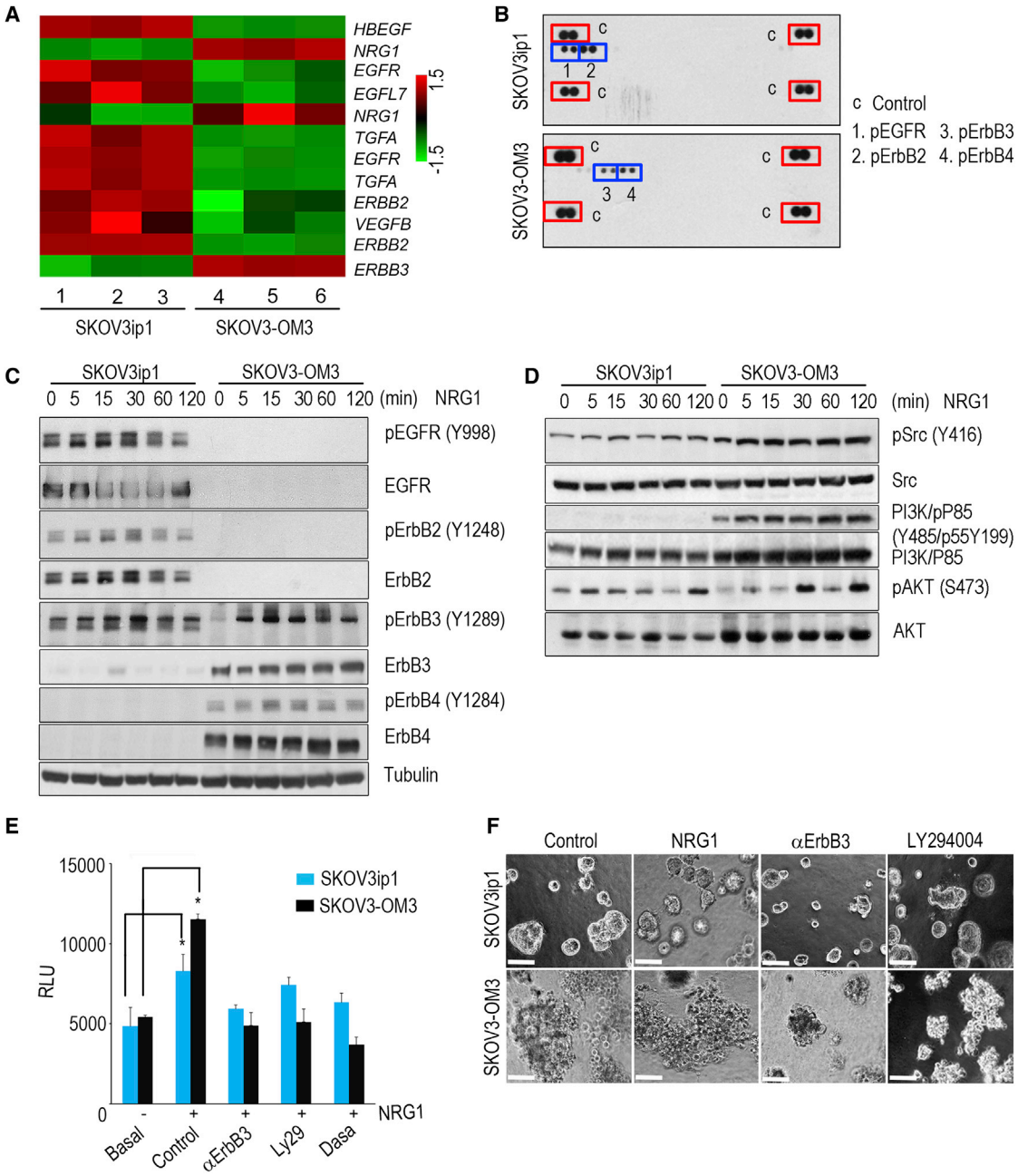


**Figure 2. Activated ErbB3/NRG1 Axis Promotes Hematogenous Ovarian Cancer Metastasis**

(A) Heat map represents normalized gene expression levels obtained from the microarray data of ovarian cancer cell lines SKOV3ip1 and SKOV3-OM3. Module of EGFR family genes differentially expressed in the SKOV3ip1 and SKOV3-OM3 cells.

(B) Phospho-RTK arrays probed with SKOV3ip1 and SKOV3-OM3 cell lysates. The red rectangles indicate the control, and blue rectangles show EGF family receptors.

(C) Immunoblot of total and phosphorylated (p) EGF receptors in SKOV3ip1 and SKOV3-OM3 cell lysates. Serum-starved SKOV3ip1 (left) and SKOV3-OM3 cells (right) were either treated with NRG1 (50 ng/ml) for different times or left untreated. Phosphorylation of EGF family receptors was determined using Western blotting with the indicated antibodies.

(D) Phosphorylation of Src and PI3k/AKT was determined using Western blotting with the indicated antibodies in SKOV3ip1 and SKOV3-OM3 cell lysates.

(E) Rac1 activation by NRG1 was measured by using a G-LISA kit. Data are represented in relative luminescence units (RLU). SKOV3ip1 and SKOV3-OM3 cells were serum starved for 24 hr; treated with antiErbB3 antibody (10 μg/ml), PI3K inhibitor (LY29004 μg/ml), or Src inhibitor (dasatinib [Dasa] 100 nM); and then stimulated with NRG1 (50 ng/ml) for 30 min. Mean ± SEM values are shown. *$p < 0.05$.

(F) Phase contrast micrographs of 4-day 3DlrBM cultures of SKOV3ip1 and highly malignant SKOV3-OM3 cells. Inhibition of ErbB3 and PI3K restored the polarity of SKOV3-OM3 cells compared with untreated control.

Scale bars represent 50 μm. See also Figure S2 and Table S2.

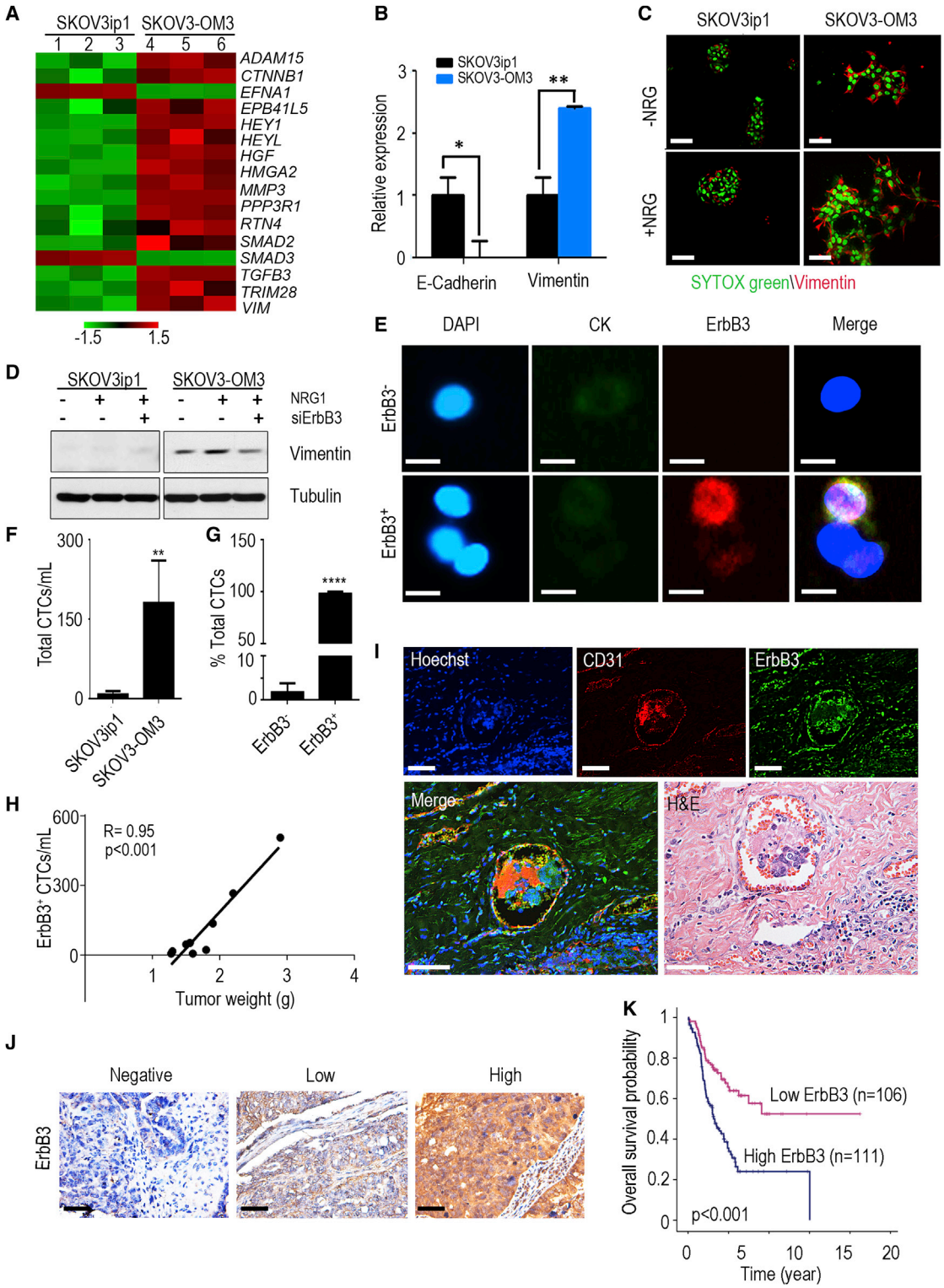


**Figure 3. ErbB3/NRG Causes Mesenchymal Transition and Promotes CTCs**

(A) Heat map from the microarray data shows that a group of genes involved in EMT were altered in SKOV3-OM3 cells compared with parental SKOV3ip1 cells. Heat map was generated to compare fold changes in the expression of genes between SKOV3ip1 and SKOV3-OM3 cells.

(B) qRT-PCR for markers of EMT in SKOV3ip1 and SKOV3-OM3 cells.

(C) Four-day 3DlrBM cultures of SKOV3ip1 and SKOV3-OM3 cells were stained with vimentin and SYTOX green. Scale bars represent 100 μm.

(D) Cell lysates of SKOV3ip1 and SKOV3-OM3 cells were immunoblotted against vimentin.

*(legend continued on next page)*

(DOPC) nanoliposomal platform, we first sought to determine whether silencing tumoral expression of ErbB3 could disrupt omental metastasis. siRNA knockdown efficiency of human (Figures S4A and S4B) and mouse (Figures S4C and S4D) specific sequences was evaluated at both the mRNA and protein levels in vitro. Sequence number 2 was selected for all subsequent human and mouse ErbB3 siRNA experiments. Tumor cells (SKOV3-OM3 and IG10-OM2) were administered via intracardiac injection, and mice were subsequently randomized to one of two treatment groups (10 mice/group): control siRNA-DOPC or ErbB3 siRNA-DOPC. The SKOV3-OM3 model was treated with human ErbB3 siRNA-DOPC, and the IG10-OM2 syngeneic model was treated with murine ErbB3 siRNA-DOPC. In the SKOV3-OM3 model, we used luciferase-labeled cells such that tumor growth and metastasis were evaluated using weekly bioluminescence imaging (Figures 4A and 4B). We found that the rate of tumor establishment in the omentum was significantly lower in the ErbB3 siRNA-DOPC group than in the control siRNA-DOPC group in both the SKOV3-OM3 (10% versus 80%; Figures 4C and 4D) and IG10-OM2 models (20% versus 60%; Figures S4E and S4F). ErbB3 silencing resulted in substantially decreased tumor growth and metastatic nodules in both models (Figures 4E and 4F). Tumoral ErbB3 expression was significantly decreased in the group treated with ErbB3 siRNA-DOPC compared with the control siRNA-DOPC-treated group (data not shown). Of note, there were no significant differences in the mean mouse weight between any of the treatment groups. To exclude possible off-target effects of siRNAs, we performed similar experiments with additional human (Figures S4G and S4H) and mouse (Figures S4I and S4J) siRNA sequences targeted against ErbB3, and the results were consistent with our prior findings.

To further characterize the role of ErbB3 in hematogenous omental metastasis from the primary tumor site, we injected tumor cells into the ovary of host parabiont mice. The mice were then randomized into two groups: (1) control siRNA-DOPC and (2) ErbB3 siRNA-DOPC. Metastatic burden was assessed at necropsy in guest mice. ErbB3 silencing significantly decreased the metastatic spread to the omentum in guest mice (Figures 4G–4I), compared with respective control groups.

We next assessed the ability of an anti-ErbB3 ectodomain-directed monoclonal antibody, MM121 (Heintz et al., 2006; Schoeberl et al., 2010), to disrupt hematogenous metastasis of ovarian cancer. MM121 binds with high affinity to ErbB3 and blocks the binding of its ligand, NRG1, thereby inhibiting its phosphorylation. Mice were treated with MM121 after intracardiac injection of SKOV3-OM3-luc cells, and bioluminescence imaging was performed at 4-day intervals (Figure 5A). MM121 treatment led to significant reduction in total tumor burden (Figure 5B). The mice were euthanized after 28 days and were necropsied to assess metastatic burden. MM121 significantly inhibited tumor growth (Figure 5C) and number of tumor nodules (Figure 5D) compared with the control group. Importantly, treatment with MM121 led to marked reductions in the frequency of omental and mesenteric metastases (Figure 5E). These biological effects are consistent with results obtained using ErbB3-targeted siRNAs. To further determine the role of ErbB3 in hematogenous omental metastasis from the primary tumor site, we injected tumor cells into the ovaries of host parabiont mice. Similar to the results described above, MM121 treatment significantly decreased the metastatic spread to the omentum in guest mice (Figure 5F) when compared with the control group. The metastatic distribution is shown in Figure 5G.

To assess the effects of ErbB3 silencing in additional models, we repeated the parabiosis experiment using the OVCA432 high-grade serous ovarian cancer model. Similar to the results obtained in the SKOV3-OM3 model, there was a significant reduction in the formation of omental metastasis in the ErbB3 siRNA-DOPC treatment group compared with control-siRNA DOPC group (Figures 5H and 5I). ErbB3 siRNA-DOPC treatment also significantly reduced tumor burden in the omentum following intracardiac injection of OVCA432 cells (Figures S5A and S5B).

Next, we wondered whether ErbB3 might be required for omental metastasis for other cancer types. To address this question, we first established colon cancer models by intracardiac injection of high ErbB3-expressing HCT116 and SW620 colon cancer cells. Mice were randomized to either control siRNA-DOPC or ErbB3 siRNA-DOPC treatment groups. Forty-five days after tumor injection, a necropsy was performed. Similar to the results obtained with the ovarian cancer model, tumor burden in the omentum was significantly reduced following ErbB3 silencing in both of these models (Figures S5C–S5F).

## ErbB3 Expression Promotes Hematogenous Omental Metastasis

To determine whether ectopic expression of ErbB3 in ErbB3 null ovarian cancer cells (HeyA8; Figure S6A) could promote hematogenous metastasis, we generated pCDH-mock (HeyA8-EV) and pCDH-ErbB3 stably transfected HeyA8 (HeyA8-ErbB3) cells. *ErbB3* expression was validated via qRT-PCR in transfected cells (Figure S6B). Three weeks following intracardiac injection of these cells into nude mice, metastatic burden was assessed at necropsy (Figure 6A). We found that 60% of mice injected with ErbB3-expressing HeyA8 cells developed omental

(E) Representative images show ErbB3$^+$, CK$^+$, and CK$^-$ CTCs within the microchannel in both SKOV3ip1 and SKOV3-OM3 in vivo models. Scale bars represent 10 μm.
(F) Quantitative representations of total CTCs in the SKOV3ip1 and SKOV3-OM3 models.
(G) ErbB3$^+$ CTCs in the SKOV3-OM3 in vivo model.
(H) Correlation of total tumor burden with enumeration of ErbB3$^+$ CTCs in mice. Aggregate metastatic burden was determined by Pearson's correlation using the aggregate tumor mass, and the number of CTCs was plotted for those specific samples.
(I) Human omental sections stained for ErbB3 and CD31 show tumor cells within blood vessels. The adjacent slide was also stained with H&E. Scale bars represent 50 μm.
(J) Representative immunohistochemical images of human ovarian tumors with low or high expression of ErbB3. Scale bars represent 50 μm.
(K) Kaplan-Meier curves of disease-specific mortality for patients with epithelial ovarian carcinoma (n = 217) based on ErbB3 expression. The log-rank test (two-sided) was used to compare differences between groups. Mean ± SEM values are shown.
*p < 0.05; **p < 0.01; ****p < 0.0001. See also Figure S3 and Tables S3 and S4.

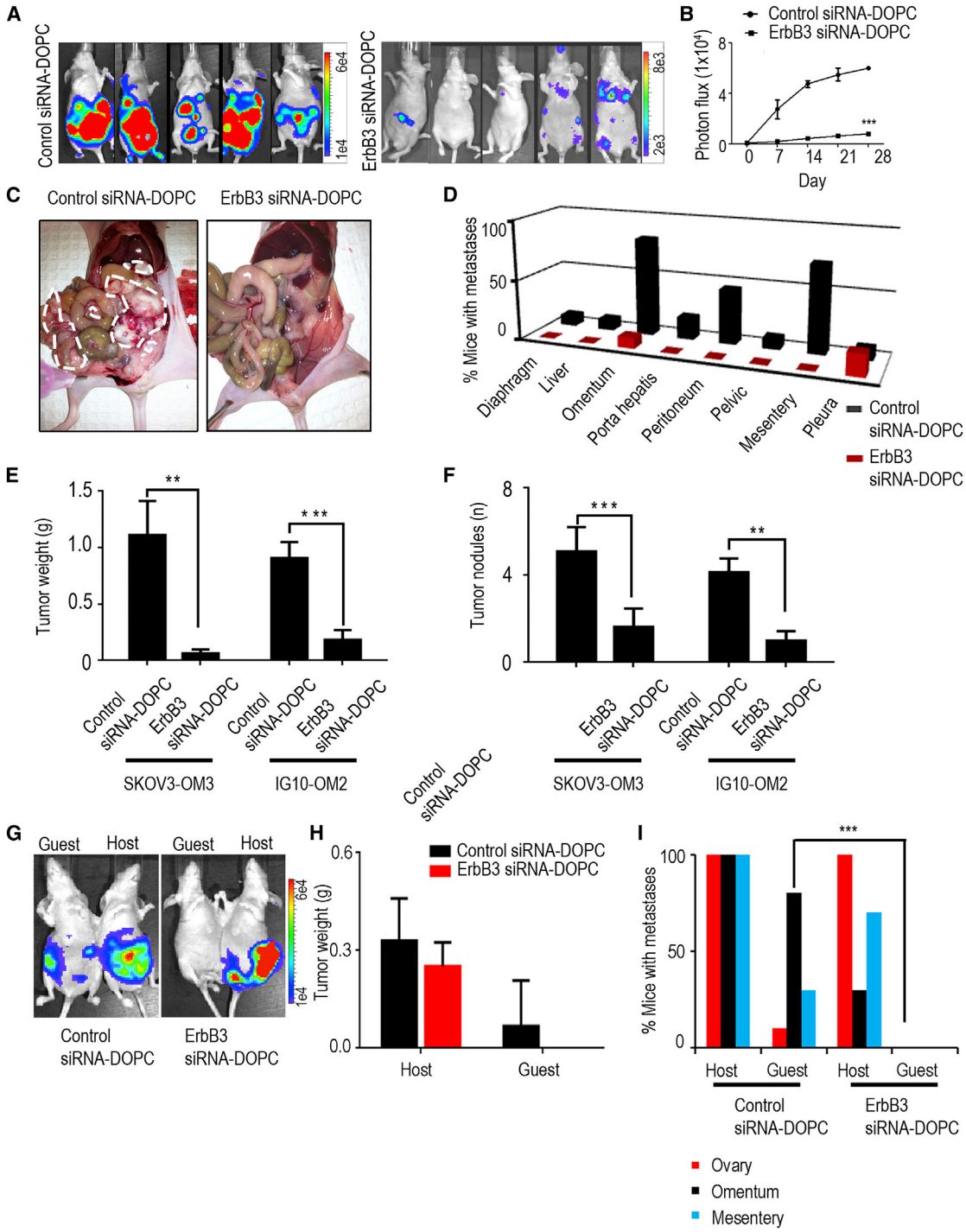


**Figure 4. Knockdown of ErbB3 Reduces Tumor Growth and Metastasis in Vivo**

(A) Nude mice that received intracardiac injections of SKOV3-OM3 cells were randomly assigned to one of two groups (control siRNA-DOPC or ErbB3 siRNA-DOPC). Bioluminescence imaging was performed on day 28. The color scale bars depicting the photon fluxes emitted from the tumor cells are shown.

(B) Quantitative representation of bioluminescence.

(C) Representative images of the extent of metastatic spread in control versus ErbB3 siRNA-DOPC-treated mice. Metastatic areas are outlined with dotted white lines.

(D) Bar graph shows the percentage of animals in each study arm with metastases to intraperitoneal and distant organ sites.

(E and F) The average tumor weight (E) and number of tumor nodules (F) are shown for SKOV3-OM3 and IG10-OM2 models 50 days after intracardiac injection.

(G) SKOV3-OM3 cells were injected into the ovary of host parabiont mice; 5 weeks later the mice were imaged using bioluminescence imaging.

(H) Tumor weight was plotted after ErbB3 siRNA-DOPC treatment.

(I) The percentage of animals in each study arm with metastases to intraperitoneal and distant organ sites was plotted. Mean ± SEM values are shown.

*p < 0.05; **p < 0.01; ***p < 0.001. See also Figure S4.

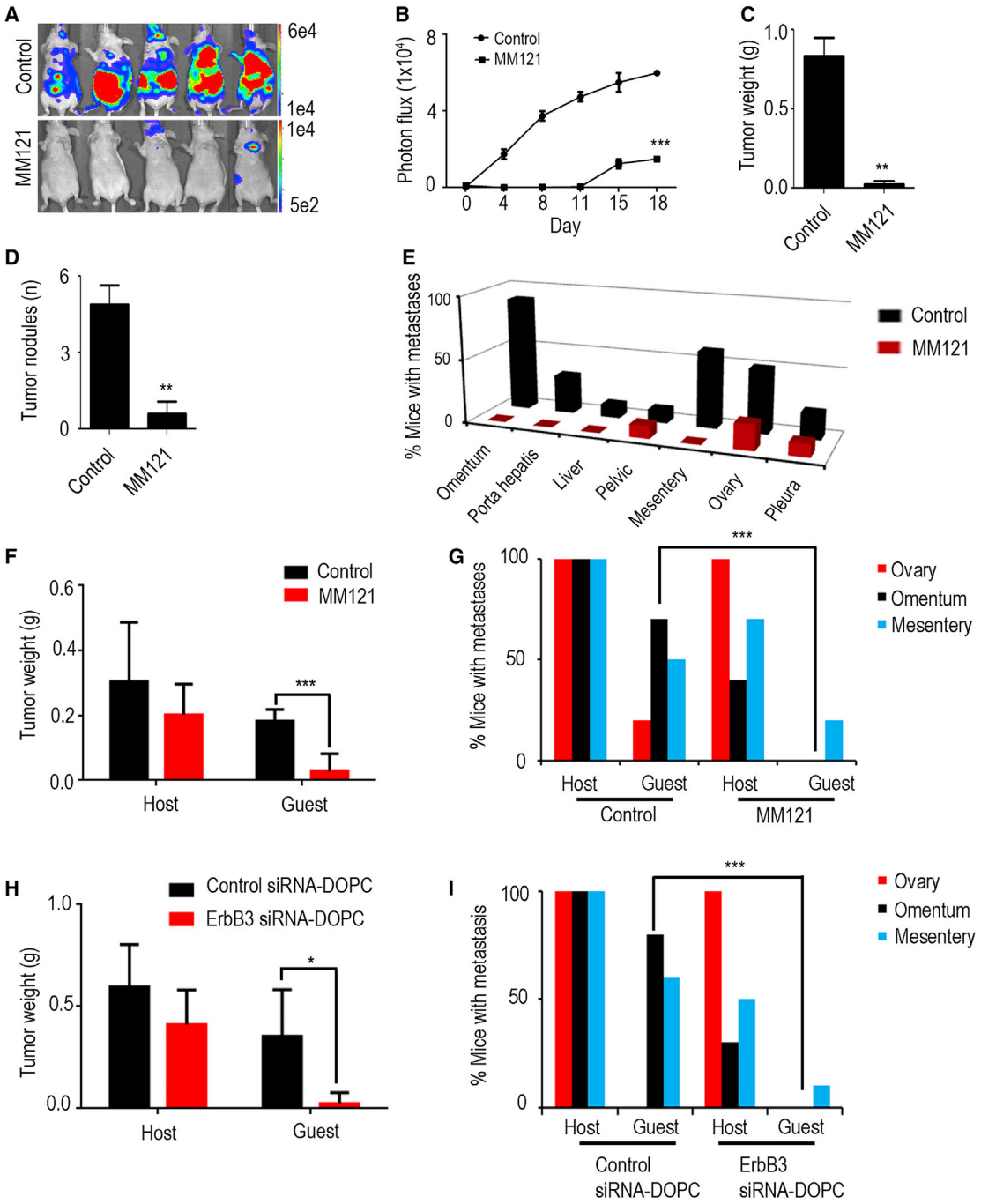


**Figure 5. Antibody-Mediated Perturbation of ErbB3 Inhibits Ovarian Cancer Metastasis**

(A) Nude mice that received intracardiac injection of SKOV3-OM3-Luc cells were randomly assigned to one of two groups (10 mice per group): group 1 was administered control (phosphate-buffered saline), and group 2 received the MM121 antibody. Bioluminescence imaging was performed on day 28. The color scales depicting the photon fluxes emitted from the tumor cells are shown.

(B) Quantitative representation of bioluminescence.

(C and D) At the end of the study, mice were euthanized, tumors were harvested, and the average tumor weight and number of nodules are shown.

(E) Bar graph shows the percentage of animals in each study arm with metastases to intraperitoneal and distant organ sites.

(F) Tumor weight in both host and guest mice were plotted after control or MM121 treatment.

(G) Percentages of mice with metastases in distant organs in host and guest mice were plotted.

(H) OVCA432 cells were injected into the ovary of host mice. Tumor weight in both host and guest mice were plotted after control siRNA-DOPC or ErbB3 siRNA-DOPC treatment.

(I) Percentage of mice with metastases in distant organs in host and guest mice. Mean ± SEM values are shown.

*$p < 0.05$; **$p < 0.01$; ***$p < 0.001$. See also Figure S5.

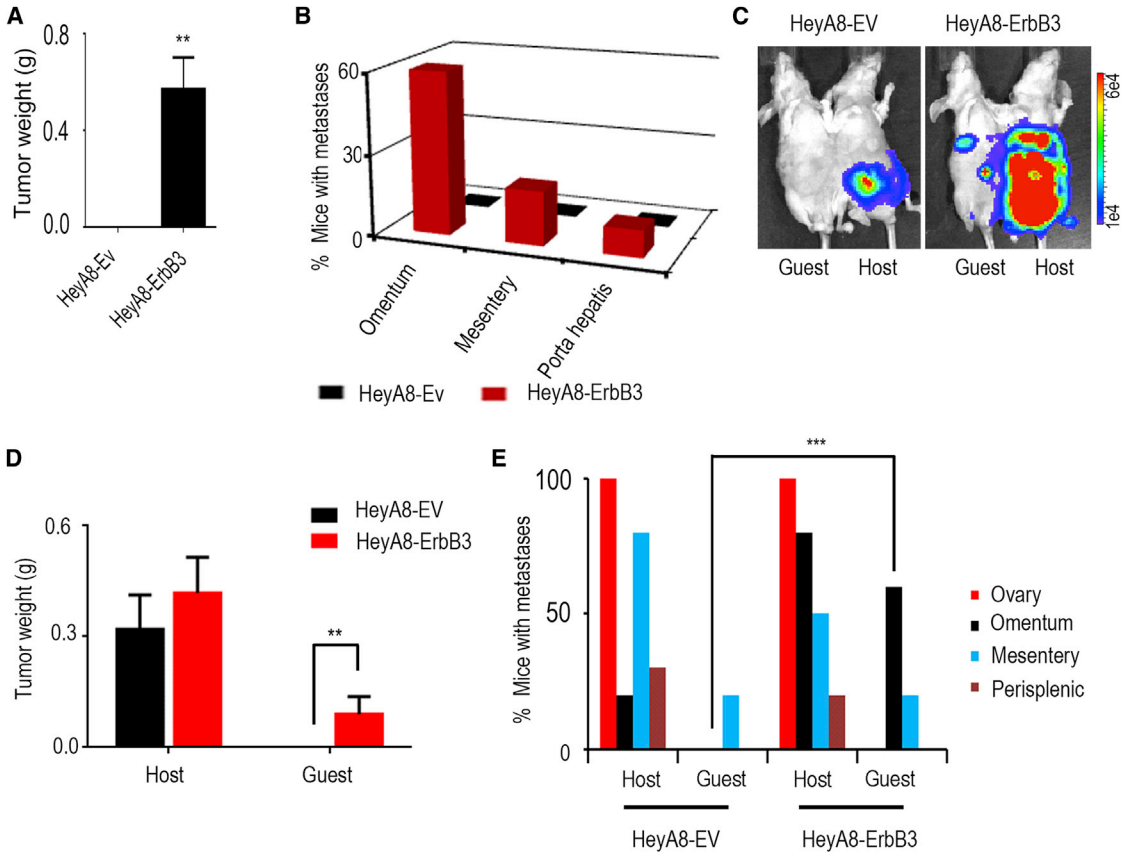


**Figure 6. ErbB3 Expression Promotes Hematogenous Omental Metastasis**

(A) Nude mice that received intracardiac injections of either HeyA8-EV or HeyA8-ErbB3 cells were necropsied after 3 weeks. Tumor weights in both groups were plotted.

(B) Percentage of mice with metastases in different organs.

(C) Bioluminescence imaging after HeyA8-EV and HeyA8-ErbB3 cell injection into the host ovary.

(D) Quantification of tumor weight at necropsy.

(E) Pattern of metastases in host and guest mice.

Mean ± SEM values are shown. **p < 0.01; ***p < 0.001. See also Figure S6.

tumors, whereas none of the mice with HeyA8 injection developed tumors in the omentum (Figure 6B; Figure S6C). We also examined the effects of ectopic ErbB3 expression on hematogenous omental metastasis from the primary site. Following injection of HeyA8-EV-Luc or HeyA8-ErbB3-Luc cells directly into the ovary in the host parabiont mice, bioluminescence imaging was carried out to monitor tumor growth in the guest mice (Figure 6C). Metastatic burden was assessed at necropsy in the guest mice (Figure 6D). Although 60% of guest mice in the HeyA8-ErbB3 group developed tumors in omentum, none of the guest mice in the HeyA8-Ev group developed omental tumor (Figure 6E; Figure S6D).

## ErbB3/NRG1 Axis Plays a Functional Role in Hematogenous Ovarian Cancer Metastasis

Having established the role of ErbB3 on omental metastasis of cancer cells, we next examined potential mechanisms underlying this phenomenon. We first examined the downstream effects of ErbB3 blockade in omental tumors. Significant reductions in the number of Ki67-positive cells were observed in omental tumors in mice treated with ErbB3 siRNA-DOPC compared with those treated with control siRNA-DOPC (Figure S7A). An increase in the number of apoptotic cells was also observed in omental tumors for mice treated with ErbB3 siRNA-DOPC. This effect of ErbB3 knockdown on cell proliferation, however, was not observed in vitro. We found that there was no significant difference in cell proliferation rate after ErbB3 silencing in SKOV3-OM3, OVCA432, or HeyA8-ErbB3 cells (Figures 7A–7C). This discrepancy between in vitro and in vivo observations prompted us to investigate whether the tumor microenvironment in the omentum provides certain stimuli that result in high level of dependency of cancer cells to the ErbB3 signaling pathway. Because NRG1 is present at a much higher level in the omentum compared with majority of the other organs (Figures S7B–S7E), we hypothesized that the effect of ErbB3 on cell proliferation is dependent on the level of NRG1 present. To test this hypothesis, we injected tumor cells subcutaneously into mice and monitored their growth following siRNA treatments. No significant difference in tumor growth rate was observed between control and ErbB3 siRNA treatment groups in this setting (Figure 7D). Ki67

staining of the tumor tissues also revealed that cell proliferation rate was minimally affected by ErbB3 knockdown in the subcutaneous site where NRG1 expression is low (Figure 7E).

The NRG1-induced cell dependency on ErbB3-mediated cell survival pathway prompted us to hypothesize that the presence of high NRG1 levels in the omentum promotes the growth of ErbB3$^+$ cancer cells. To examine this, we used the soft agar assay with HeyA8-ErbB3 cells in the presence or absence of NRG1 (Figure 7F). The average colony size in NRG1 treatment group was >3-fold larger compared with those with no NRG1 treatment, indicating the role of NRG1 in promoting the growth of ErbB3$^+$ cells (Figure 7G). Importantly, HeyA8-Ev cells did not form sizable colonies even in the presence of NRG1. We found that NRG1 expression was higher in the periendothelial environment of the human omentum than in peripheral fat vasculature (Figure S7F). We also examined NRG1 expression in human primary ovarian tumors. NRG1 expression was evident in both stromal and cancer cells in all 11 tumors examined (Figures S7G and S7H). To further investigate the role of the NRG1/ErbB3 axis in omental metastasis, we silenced NRG1 expression in mice by using a mouse-specific NRG1 siRNA incorporated in chitosan nanoparticles (NRG1 siRNA-CH). The ability of these chitosan nanoparticles to deliver siRNAs to tumor stroma has been previously demonstrated (Han et al., 2010; Lu et al., 2010). Effective silencing of NRG1 was observed in omentum following NRG1 siRNA-CH compared with control siRNA-CH (Figure S7I). In this experiment, all mice received intracardiac injection of SKOV3-OM3 cells. At week 4, the animals were sacrificed, and necropsy was performed. NRG1 silencing significantly reduced the formation of omental metastasis by SKOV3-OM3 cells when compared with the control siRNA-CH-treated group (Figures 7H and 7I). To evaluate for the presence of any micrometastases in the omentum in both treatment groups, we performed H&E staining on paraffin sections of the omentum. Omental metastases were significantly reduced in the NRG1 siRNA-CH treatment group (Figure 7J). Similar results were obtained when HeyA8-ErbB3 cells were used (Figures 7K and 7L).

## DISCUSSION

In the current study, we have demonstrated a previously unrecognized paradigm for ovarian cancer metastasis in which ovarian cancer cells metastasize hematogenously with a strong predilection for the omentum (Figure 8). We discovered that this tropism relies on the ErbB3/NRG1 signaling axis, whereby pathway disruption leads to a substantial reduction in the metastatic spread of this disease. Mechanistically, the omental vascular microenvironment promotes this selectivity by overexpressing the ligand and target relative to other potential metastatic sites. Given that the expression of ErbB3 is independently prognostic for overall survival among ovarian cancer patients, these observations provide an important advance in customizing therapeutic interventions for women with ovarian cancer.

The primary therapeutic challenge with advanced stage ovarian cancer is that it is characterized by global genomic instability (Cancer Genome Atlas Research Network, 2011). Thus, it is not surprising that no single target has been successfully leveraged for durable survival. Nevertheless, understanding the components driving the metastatic milieu can have a practical impact on contemporary management. As we describe here, ErbB3 was detected on most of the CTCs collected from ovarian cancer patients. Because they can be serially measured in surveillance of patients either in remissive states or at high risk for the development of cancer, a vector change from baseline may prove an informative biomarker for cancer recurrence or occurrence, respectively. Similarly, based on our observations, we would expect that the omental "soil" could be made more hostile for future tumor implantation by post-treatment maintenance anti-ErbB3 therapy. Indeed, this strategy has proved fruitful in many settings such as the use of bevacizumab, nintedanib, and pazopanib in women responding to front-line and/or recurrent platinum-based chemotherapy (Aghajanian et al., 2012; Burger, 2011; Perren et al., 2011), cediranib in women with platinum-based chemotherapy for recurrent ovarian cancer (Ledermann et al., 2013), and paclitaxel (Markman and Walker, 2006). Currently, the human monoclonal anti-ErbB3 antibody, MM121, is in clinical development and provides an opportunity to test this hypothesis. Of note, a recently reported randomized phase II trial of paclitaxel with or without concomitant MM121 in patients with recurrent platinum-resistant ovarian cancer did not indicate a distinct benefit for the combination (Merrimack Pharmaceuticals, 2013). However, based on our findings, selective targeting of ErbB3 would perform better as a preventative or maintenance strategy. Nevertheless, a select biomarker-derived cohort may be identified as an alternative candidate for this therapy. This has been hypothesized in other trials of ErbB family targeting in ovarian cancer, such as pertuzumab (Gordon et al., 2006). This targeted agent prevents ErbB2 dimerization. Although it did not provide superior progression-free survival in a placebo-controlled randomized phase II trial in combination with gemcitabine among unselected platinum-resistant ovarian cancer patients, a post hoc analysis of ErbB2 and ErbB3 activity at the mRNA and protein level did suggest pertuzumab was increasingly more active the lower the activity of ErbB3 (Amler, 2010). Formal clinical testing of this hypothesis is underway in breast (NCT01918254) and ovarian (NCT01684878) cancer. Further clinical evaluation of ErbB3 targeting in ovarian cancer is warranted, including the assessment of different therapeutic strategies in selected patients based on tumor or CTC ErbB3 expression.

Collectively, our data provide an understanding of the mechanisms underlying ovarian cancer metastasis whereby ErbB3 plays a critical role in hematogenous dissemination of ovarian cancer to the omentum. Our complete understanding of this metastatic pathway will open rational avenues for therapeutic interventions in ovarian cancer patients.

## EXPERIMENTAL PROCEDURES

### Cell Lines and Culture

The derivation and source of the human ovarian cancer cell lines were previously described (Apte et al., 2004). These cells and their subpopulations were maintained in RPMI 1640 supplemented with 15% fetal bovine serum and 0.1% gentamicin sulfate (Gemini Bioproducts). IG10 cells (a gift from Dr. Katherine Roby, University of Kansas Medical Center) and their subpopulations were maintained in Dulbecco's modified Eagle's medium-F12 supplemented with 5% fetal bovine serum, 1× insulin-transferrin-sodium selenite supplement (Roche Diagnostics), and 0.1% gentamicin sulfate. All cell lines

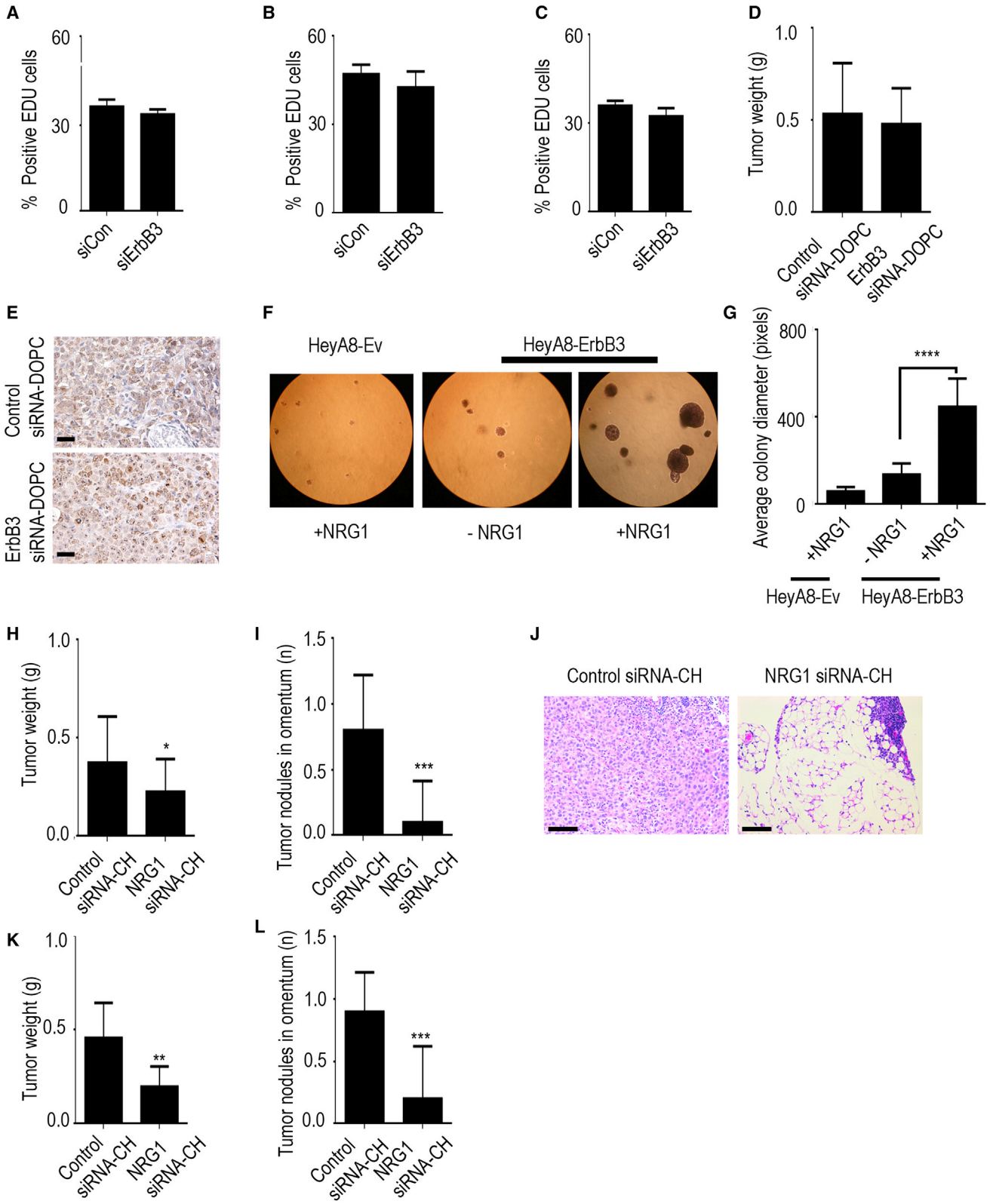


**Figure 7. NRG1 Activates ErbB3 Signaling and Enhances Omental Metastasis**

(A–C) Percentage of EDU-positive SKOV3-OM3 (A), OVCA432 (B), or HeyA8-ErbB3 (C) cells treated with either control siRNA (siCon) or ErbB3 siRNA (siErbB3). (D) SKOV3-OM3 cells were injected subcutaneously and treated with either control siRNA-DOPC or ErbB3 siRNA-DOPC for 4 weeks.

*(legend continued on next page)*

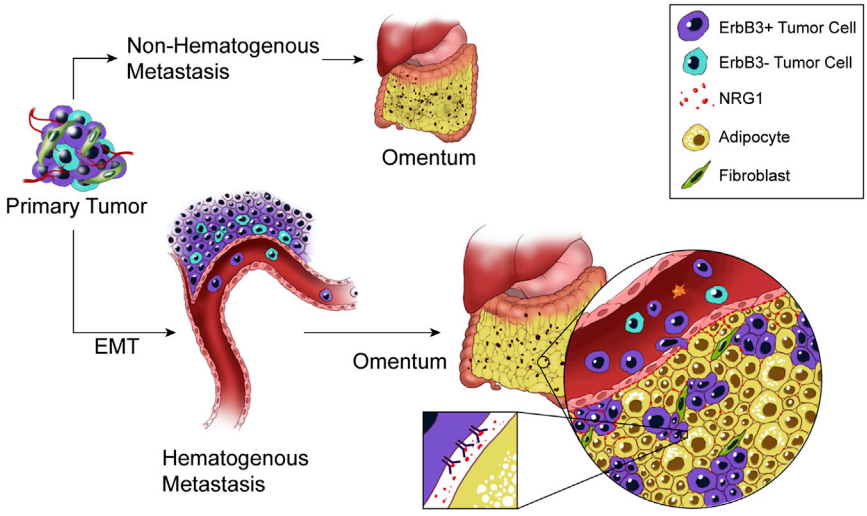


**Figure 8. Model of Ovarian Cancer Metastasis to Omentum**

(Top) Schematic representation of nonhematogenous metastasis to the omentum. Traditionally, epithelial ovarian cancer is thought to metastasize via direct surface spread.

(Bottom) Our results point to an alternative pathway that also involves hematogenous metastasis with strong tropism toward the omentum.

were routinely screened for mycoplasma and pathogenic viruses (Fisher). All experiments were performed with cell cultures at 60%–80% confluence.

### Microarray

Total RNA was extracted from the cell lines using a mirVana RNA isolation labeling kit (Ambion). We used 500 ng of total RNA for labeling and hybridization, according to the manufacturer's protocols (Illumina). After the bead chips were scanned with an Illumina BeadArray Reader (Illumina), the microarray data were normalized, and log2 values were transformed in R. The heat map was generated using R analysis and Netwalker. We ranked the fold change between SKOV3-OM3 and SKOV3ip1 cells and developed a network of the 350 most altered genes that were either down- or upregulated. We used a network-based approach on the premise that changes in phenotype and cellular behavior are driven by pathways and networks (Komurov et al., 2012a). This approach allowed us to rapidly identify gene sets that are functionally related and form interactions or networks that can drive the biological process.

### Human Phospho-RTK Array

A human phospho-RTK array (R&D Systems #ARY001), which is more sensitive than immunoprecipitation analysis, was used to detect the simultaneous expression of tyrosine-phosphorylated RTKs. This array contains 42 RTK capture antibodies spotted in duplicate. SKOV3ip1 and SKOV3-OM3 cell lysates (50 μg) were incubated with the membrane overnight in the buffer according to the manufacturer's protocol; the array was performed as previously described (Hou et al., 2011). We used the anti-phosphotyrosine horseradish peroxidase detection antibody to capture the expression of phosphorylated tyrosine residues on activated receptors.

### Plasmids and Transfections

Cells were transfected with Lipofectamine 2000 reagent (Invitrogen) using siRNAs (Sigma-Aldrich) according to the manufacturer's protocol. ErbB3 overexpressing HeyA8 cells were generated using pDONR223 plasmid. See Supplemental Experimental Procedures for additional details.

### G-LISA

Rac1 activation in SKOV3ip1 and SKOV3-OM3 cells was determined using a Rac1-activation G-LISA (Cytoskeleton). Cells grown to 70% confluency in tissue culture Petri dishes were serum starved overnight. The cells were cultured as indicated and stimulated with NRG1 for 30 min. Subsequently, cells were washed with PBS, resuspended in lysis buffer, and harvested. Total protein concentration was determined using protein assay reagent. The G-LISA contains a Rac1-GTP-binding protein immobilized on microplates. Bound active Rac1 was detected with a specific antibody and luminescence. The luminescence signal was quantified using a microplate reader (SpectraFluor Plus, Tecan).

### Liposomal Nanoparticle Preparation

siRNAs for in vivo delivery were incorporated into DOPC nanoliposomes as previously described (Landen et al., 2005; Pecot et al., 2013; Thaker et al., 2004). DOPC and siRNA were mixed in the presence of excess tertiary butanol at a ratio of 1:10 (w/w) siRNA/DOPC. Tween 20 was added to the mixture in a ratio of 1:19 Tween 20: siRNA/DOPC. The mixture was vortexed, frozen in an acetone/dry ice bath, and lyophilized. Before in vivo administration, this preparation was hydrated with PBS at room temperature at 5 μg in 200 μl of PBS per injection. siRNAs were incorporated into chitosan nanoparticles as described previously (Lu et al., 2010; Stone et al., 2012).

### Animal Studies

All animal work was performed in accordance with protocols approved by the M.D. Anderson Institutional Animal Care and Use Committee. Female athymic nude (NCr-nu) and immunocompetent (C57BL/6) mice (5–8 weeks) were purchased from the Animal Production Area of the National Cancer Institute-Frederick Cancer Research and Development Center and maintained as previously described (Lee et al., 2012).

### Parabiosis Model

To identify the biological role of ovarian CTCs, we used a parabiosis model system with both immunocompetent (C57BL/6) and immunodeficient (nude) mice that underwent parabiotic surgery. Briefly, anesthetized mice (0.5 mg of pentobarbital/g of body weight; Abbott Laboratories) were cleaned, and incisions were made from the humerus to the femur. The skin of the two mice was then anastomosed. We took care during the experiments to avoid twisting by using a flexible cohesive veterinarian bandage (1-inch width, catalog number COFLEX1; Med-Vet International). Two weeks later, Evan's blue dye was

(E) Ki67 staining on subcutaneous tumor sections. Scale bars represent 100 μm.
(F) HeyA8-Ev and HeyA8-ErbB3 cells on soft agar in the presence or absence of NRG1.
(G) Quantification of the average colony size from experiment shown in (F).
(H) Nude mice were treated with control siRNA-CH or NRG1 siRNA-CH nanoparticles and injected with SKOV3-OM3 cells. Aggregate tumor weight was assessed 4 weeks later.
(I) The average number of tumor nodules in the omentum was plotted.
(J) H&E staining on omental sections after siRNA treatments. Scale bars represent 100 μm.
(K and L) Nude mice were treated with control siRNA-CH or NRG1 siRNA-CH nanoparticles and injected with HeyA8-ErbB3 cells into the heart. Three weeks later, the mice were necropsied. Aggregate tumor weight (K) and number of nodules in the omentum (L) were plotted.
Mean ± SEM values are shown. *$p < 0.05$; **$p < 0.01$; ***$p < 0.001$; ****$p < 0.0001$. See also Figure S7.

injected into the tail vein of one of the parabionts to confirm common circulation (Kim et al., 2009). Specifically, 2 weeks after anastomosis, the host mice were injected with tumor cells either into the peritoneal cavity or directly into the ovary. The host mice typically survived for 28–35 days. Guest mice showed luciferase signal after 45 days. We observed the guest mice for up to 3 months.

### In Vivo Model of Ovarian Cancer and Tissue Processing

SKOV3-OM3 and IG10-OM2 ($1 \times 10^6$) cells were transduced with lentivirus-encoding luciferase and used for intracardiac injection of nude or C57BL/6 mice, respectively. To knock down ErbB3 expression, we used either siRNA (150 μg/kg of body weight; 2 times/week; intraperitoneally) or MM121 antibody/SAR256212 (being codeveloped by Merrimack Pharmaceuticals and Sanofi) (30 mg/kg of body weight; 3 times/week; intraperitoneally). To study the reverse, we ectopically expressed ErbB3 in HeyA8 cells and injected them into nude mice (intracardiac, $2.5 \times 10^5$). The mice were imaged once weekly for bioluminescence signal using a Xenogen IVIS system. At the time of necropsy, the weight, number, and distribution of tumors were recorded. Individuals who performed necropsies were blinded to the treatment group assignments. Tissue specimens were fixed with either formalin or optimal cutting temperature compound (OCT; Miles) or snap-frozen in liquid nitrogen. Staining was performed in formalin-fixed, paraffin-embedded 8-μm-thick tumor sections, or OCT-embedded frozen tissue sections. See Supplemental Experimental Procedures for additional details.

### Blood Collection

Nude mice were injected with SKOV3ip1 or SKOV3-OM3 ($1x10^6$) cells intraperitoneally. Twenty-five days after cell injection, 500 μl of blood was collected via cardiac puncture into Eppendorff tubes containing 500 μl of anti-clumping reagent (CEE-Sure; Biocept). Blood samples were processed in Biocept's College of American Pathologists-accredited laboratory. A detailed description of CTC capture and immunofluorescence imaging was previously described (Pecot et al., 2011). Each microchannel was scored for the presence of CTCs on the basis of standard staining criteria ($CK^{+/-}CD45^{-}/DAPI^{+}/ErbB3^{+/-}$).

### Patient-Derived Samples

After informed consent, blood samples were drawn from patients with ovarian tumors according to an Institutional Review Board-approved protocol at M.D. Anderson Cancer Center, where the patients were being treated. These cells were maintained in tissue culture for 14 days, cytospun, and stained for ErbB3 expression.

### Tissue Microarray

After approval by the Institutional Review Board, patient tissue microarray blocks were constructed by taking core samples from morphologically representative areas of paraffin-embedded tissues and assembling them on a recipient paraffin block with a precision instrument (Beecher Instruments) as described previously (Merritt et al., 2008). The final tissue microarray consisted of 3 blocks with 217 available samples. ErbB3 expression was determined by semiquantitatively assessing the percentage of stained tumor cells using the protocol described previously (Merritt et al., 2008). Briefly, the stained slides were scored on the basis of their immunohistochemical score (high expression, >100; low expression, ≤100) (McCarty et al., 1985; Singh et al., 2007).

### Statistical Analysis

The data are presented as means ± SD. Statistical comparisons between experimental groups were analyzed by unpaired Student's t test, and a two-tailed $p < 0.05$ was taken to indicate statistical significance. For analyzing the correlation, we used Pearson, and the p values are indicated. We used Fisher's exact test to analyze the differences in the incidence of metastases relative to controls. We analyzed patient survival using the Kaplan-Meier method and compared the curves using a log rank (Mantel-Cox) test.

## ACCESSION NUMBERS

The microarray data have been deposited in the Gene Expression Omnibus under accession number GSE52999.

## SUPPLEMENTAL INFORMATION

Supplemental Information includes Supplemental Experimental Procedures, seven figures, and four tables and can be found with this article online at http://dx.doi.org/10.1016/j.ccr.2014.05.002.

## ACKNOWLEDGMENTS

The authors thank Donna Reynolds, Dr. Robert Langley, Cristina Ivan, and Sang-Bae Kim for helpful discussions, for providing reagents, and for help with biostatistical analyses. We also thank David Aten for help with graphics. S.Y.W. is supported by Ovarian Cancer Research Fund, Inc., Foundation for Women's Cancer, and Cancer Prevention Research Institute Texas (CPRIT) training grants (RP101502 and RP101489). B.Z. and H.J.D. are supported by NIH T32 Training Grant CA101642. P.C.R. is supported by the Ann Schreiber Program for Excellence grant from the Ovarian Cancer Research Foundation and a Scientific scholar award from the Marsha Rivkin Center for Ovarian Cancer Research. This work was also supported in part by NIH grants (P50CA083639, CA109298, P50CA098258, CA177909, U54CA151668, UH2TR000943, CA016672, U54CA96300, and U54CA96297), CPRIT RP110595 and RP120214, an Ovarian Cancer Research Fund Program Project Development Grant, Department of Defense grants (OC120547 and OC093416), the Betty Ann Asche Murray Distinguished Professorship, the Marcus Foundation, the RGK Foundation, the Gilder Foundation, the Judi A. Rees Ovarian Cancer Research Fund, the Chapman Foundation, the Meyer and Ida Gordon Foundation, the Ann Rife Cox Chair in Gynecology, and the Blanton-Davis Ovarian Cancer Research Program. We also acknowledge support from the Small Animal Imaging Facility.

Received: April 20, 2013
Revised: December 9, 2013
Accepted: May 1, 2014
Published: July 14, 2014

## REFERENCES

Adam, L., Vadlamudi, R., Kondapaka, S.B., Chernoff, J., Mendelsohn, J., and Kumar, R. (1998). Heregulin regulates cytoskeletal reorganization and cell migration through the p21-activated kinase-1 via phosphatidylinositol-3 kinase. J. Biol. Chem. *273*, 28238–28246.

Aghajanian, C., Blank, S.V., Goff, B.A., Judson, P.L., Teneriello, M.G., Husain, A., Sovak, M.A., Yi, J., and Nycum, L.R. (2012). OCEANS: A randomized, double-blind, placebo-controlled phase III trial of chemotherapy with or without bevacizumab in patients with platinum-sensitive recurrent epithelial ovarian, primary peritoneal, or fallopian tube cancer. J. Clin. Oncol. *30*, 2039–2045.

Ahmed, A.A., Lu, Z., Jennings, N.B., Etemadmoghadam, D., Capalbo, L., Jacamo, R.O., Barbosa-Morais, N., Le, X.F., Vivas-Mejia, P., Lopez-Berestein, G., et al. (2010). SIK2 is a centrosome kinase required for bipolar mitotic spindle formation that provides a potential target for therapy in ovarian cancer. Cancer Cell *18*, 109–121.

Akin, O., Sala, E., Moskowitz, C.S., Ishill, N., Soslow, R.A., Chi, D.S., and Hricak, H. (2008). Perihepatic metastases from ovarian cancer: Sensitivity and specificity of CT for the detection of metastases with and those without liver parenchymal invasion. Radiology *248*, 511–517.

Amler, L.C. (2010). HER3 mRNA as a predictive biomarker in anticancer therapy. Expert Opin. Biol. Ther. *10*, 1343–1355.

Apte, S.M., Bucana, C.D., Killion, J.J., Gershenson, D.M., and Fidler, I.J. (2004). Expression of platelet-derived growth factor and activated receptor in clinical specimens of epithelial ovarian cancer and ovarian carcinoma cell lines. Gynecol. Oncol. *93*, 78–86.

Burger, R.A. (2011). Antiangiogenic agents should be integrated into the standard treatment for patients with ovarian cancer. Ann. Oncol. *22* (*Suppl 8*), viii65–viii68.

Cancer Genome Atlas Research Network (2011). Integrated genomic analyses of ovarian carcinoma. Nature *474*, 609–615.

Castadot, P., Magné, N., Berghmans, T., Drowart, A., Baeyens, L., Smets, D., and Van Houtte, P. (2005). [Ovarian metastasis and lung adenocarcinoma: A case report]. Cancer Radiother. *9*, 183–186.

Gordon, M.S., Matei, D., Aghajanian, C., Matulonis, U.A., Brewer, M., Fleming, G.F., Hainsworth, J.D., Garcia, A.A., Pegram, M.D., Schilder, R.J., et al. (2006). Clinical activity of pertuzumab (rhuMAb 2C4), a HER dimerization inhibitor, in advanced ovarian cancer: Potential predictive relationship with tumor HER2 activation status. J. Clin. Oncol. *24*, 4324–4332.

Han, H.D., Mangala, L.S., Lee, J.W., Shahzad, M.M., Kim, H.S., Shen, D., Nam, E.J., Mora, E.M., Stone, R.L., Lu, C., et al. (2010). Targeted gene silencing using RGD-labeled chitosan nanoparticles. Clin. Cancer Res. *16*, 3910–3922.

Heintz, A.P.M., Odicino, F., Maisonneuve, P., Quinn, M.A., Benedet, J.L., Creasman, W.T., Ngan, H.Y.S., Pecorelli, S., and Beller, U. (2006). Carcinoma of the ovary. FIGO 26th Annual report on the results of treatment in gynecological cancer. Int. J. Gynaecol. Obstet. *95* (*Suppl 1*), S161–S192.

Hou, J., Dong, J., Sun, L., Geng, L., Wang, J., Zheng, J., Li, Y., Bridge, J., Hinrichs, S.H., and Ding, S.-J. (2011). Inhibition of phosphorylated c-Met in rhabdomyosarcoma cell lines by a small molecule inhibitor SU11274. J. Transl. Med. *9*, 64.

Kim, S.J., Kim, J.S., Papadopoulos, J., Wook Kim, S., Maya, M., Zhang, F., He, J., Fan, D., Langley, R., and Fidler, I.J. (2009). Circulating monocytes expressing CD31: Implications for acute and chronic angiogenesis. Am. J. Pathol. *174*, 1972–1980.

Komurov, K., White, M.A., and Ram, P.T. (2010). Use of data-biased random walks on graphs for the retrieval of context-specific networks from genomic data. PLoS Comput. Biol. *6*, e1000889.

Komurov, K., Dursun, S., Erdin, S., and Ram, P.T. (2012a). NetWalker: A contextual network analysis tool for functional genomics. BMC Genomics *13*, 282.

Komurov, K., Tseng, J.T., Muller, M., Seviour, E.G., Moss, T.J., Yang, L., Nagrath, D., and Ram, P.T. (2012b). The glucose-deprivation network counteracts lapatinib-induced toxicity in resistant ErbB2-positive breast cancer cells. Mol. Syst. Biol. *8*, 596.

Landen, C.N., Jr., Chavez-Reyes, A., Bucana, C., Schmandt, R., Deavers, M.T., Lopez-Berestein, G., and Sood, A.K. (2005). Therapeutic EphA2 gene targeting in vivo using neutral liposomal small interfering RNA delivery. Cancer Res. *65*, 6910–6918.

Ledermann, J.A.., Perren, T., Raja1, F.A., Embleton, A. C., Rustin, G.J.S., Jayson, G., Kaye, S.B., Swart, A., Vaughan, M., and Hirte, H. (2013). Randomised double-blind phase III trial of cediranib (AZD 2171) in relapsed platinum sensitive ovarian cancer: Results of the ICON6 trial. http://conference.ncri.org.uk/abstracts/2013/abstracts/ClinicalShowcase4.html.

Lee, S.J., Ghosh, S.C., Han, H.D., Stone, R.L., Bottsford-Miller, J., Shen, Y., Auzenne, E.J., Lopez-Araujo, A., Lu, C., Nishimura, M., et al. (2012). Metronomic activity of CD44-targeted hyaluronic acid-paclitaxel in ovarian carcinoma. Clin. Cancer Res. *18*, 4114–4121.

Lim, M.C., Kang, S., Lee, K.S., Han, S.-S., Park, S.-J., Seo, S.-S., and Park, S.-Y. (2009). The clinical significance of hepatic parenchymal metastasis in patients with primary epithelial ovarian cancer. Gynecol. Oncol. *112*, 28–34.

Lu, C., Han, H.D., Mangala, L.S., Ali-Fehmi, R., Newton, C.S., Ozbun, L., Armaiz-Pena, G.N., Hu, W., Stone, R.L., Munkarah, A., et al. (2010). Regulation of tumor angiogenesis by EZH2. Cancer Cell *18*, 185–197.

Markman, M., and Walker, J.L. (2006). Intraperitoneal chemotherapy of ovarian cancer: A review, with a focus on practical aspects of treatment. J. Clin. Oncol. *24*, 988–994.

McCarty, K.S., Jr., Miller, L.S., Cox, E.B., Konrath, J., and McCarty, K.S., Sr.. (1985). Estrogen receptor analyses. Correlation of biochemical and immunohistochemical methods using monoclonal antireceptor antibodies. Arch. Pathol. Lab. Med. *109*, 716–721.

Merrimack Pharmaceuticals (2013). Merrimack Pharmaceuticals Announces Results from a phase 2 study of MM-121 (SAR256212) in combination with paclitaxel in patients with platinum-resistant or refractory advanced ovarian cancers. http://investors.merrimackpharma.com/releasedetail.cfm?ReleaseID=801512.

Merritt, W.M., Lin, Y.G., Han, L.Y., Kamat, A.A., Spannuth, W.A., Schmandt, R., Urbauer, D., Pennacchio, L.A., Cheng, J.-F., Nick, A.M., et al. (2008). Dicer, Drosha, and outcomes in patients with ovarian cancer. N. Engl. J. Med. *359*, 2641–2650.

Naora, H., and Montell, D.J. (2005). Ovarian cancer metastasis: Integrating insights from disparate model organisms. Nat. Rev. Cancer *5*, 355–366.

Pecot, C.V., Bischoff, F.Z., Mayer, J.A., Wong, K.L., Pham, T., Bottsford-Miller, J., Stone, R.L., Lin, Y.G., Jaladurgam, P., Roh, J.W., et al. (2011). A novel platform for detection of CK+ and CK− CTCs. Cancer Discov *1*, 580–586.

Pecot, C.V., Rupaimoole, R., Yang, D., Akbani, R., Ivan, C., Lu, C., Wu, S., Han, H.D., Shah, M.Y., Rodriguez-Aguayo, C., et al. (2013). Tumour angiogenesis regulation by the miR-200 family. Nat. Commun. *4*, 2427.

Perren, T.J., Swart, A.M., Pfisterer, J., Ledermann, J.A., Pujade-Lauraine, E., Kristensen, G., Carey, M.S., Beale, P., Cervantes, A., Kurzeder, C., et al. (2011). A phase 3 trial of bevacizumab in ovarian cancer. N. Engl. J. Med. *365*, 2484–2496.

Phillips, K.G., Velasco, C.R., Li, J., Kolatkar, A., Luttgen, M., Bethel, K., Duggan, B., Kuhn, P., and McCarty, O.J.T. (2012). Optical quantification of cellular mass, volume, and density of circulating tumor cells identified in an ovarian cancer patient. Front Oncol *2*, 72.

Schoeberl, B., Faber, A.C., Li, D., Liang, M.-C., Crosby, K., Onsum, M., Burenkova, O., Pace, E., Walton, Z., Nie, L., et al. (2010). An ErbB3 antibody, MM-121, is active in cancers with ligand-dependent activation. Cancer Res. *70*, 2485–2494.

Singh, M., Zaino, R.J., Filiaci, V.J., and Leslie, K.K. (2007). Relationship of estrogen and progesterone receptors to clinical outcome in metastatic endometrial carcinoma: A Gynecologic Oncology Group Study. Gynecol. Oncol. *106*, 325–333.

Stone, R.L., Nick, A.M., McNeish, I.A., Balkwill, F., Han, H.D., Bottsford-Miller, J., Rupairmoole, R., Armaiz-Pena, G.N., Pecot, C.V., Coward, J., et al. (2012). Paraneoplastic thrombocytosis in ovarian cancer. N. Engl. J. Med. *366*, 610–618.

Tarin, D., Price, J.E., Kettlewell, M.G., Souter, R.G., Vass, A.C., and Crossley, B. (1984). Mechanisms of human tumor metastasis studied in patients with peritoneovenous shunts. Cancer Res. *44*, 3584–3592.

Thaker, P.H., Deavers, M., Celestino, J., Thornton, A., Fletcher, M.S., Landen, C.N., Kinch, M.S., Kiener, P.A., and Sood, A.K. (2004). EphA2 expression is associated with aggressive features in ovarian carcinoma. Clin. Cancer Res. *10*, 5145–5150.